OPEN ACCESS

University of BRISTOL

Azarpeyvand, M. (2014). Prediction of negative radiation forces due to a Bessel beam. *Journal of the Acoustical Society of America*, *136*(2), 547-555. https://doi.org/10.1121/1.4884758

Publisher's PDF, also known as Version of record

Link to published version (if available):
10.1121/1.4884758

Link to publication record in Explore Bristol Research
PDF-document

Copyright (2014) Acoustical Society of America. This article may be downloaded for personal use only. Any other use requires prior permission of the author and the Acoustical Society of America. The following article appeared in J. Acoust. Soc. Am. 136, 547 (2014) and may be found at http://dx.doi.org/10.1121/1.4884758.

University of Bristol - Explore Bristol Research
General rights

This document is made available in accordance with publisher policies. Please cite only the published version using the reference above. Full terms of use are available:
http://www.bristol.ac.uk/red/research-policy/pure/user-guides/ebr-terms/

CrossMark click for updates

Prediction of negative radiation forces due to a Bessel beam

Mahdi Azarpeyvand[a)]
Department of Mechanical Engineering, University of Bristol, Bristol BS8 1TR, United Kingdom

(Received 23 April 2013; revised 23 May 2014; accepted 5 June 2014)

The mechanism of generating backward dragging forces on objects standing in the path of a single, translationally invariant, symmetric acoustic Bessel beam is studied. This paper aims to provide mechanical and structural conditions for the emergence of negative axial forces based on the elastodynamic response of acoustically penetrable objects and beam's nonparaxiality parameter. An extensive numerical study has been performed for various liquid and solid elastic cases to illustrate the validity of the proposed eigenfrequency-based conditions. Results have revealed the existence of a complex but interpretable link between the emergence of negative radiation forces on spheres illuminated by zero-order Bessel beams and the eigenfrequencies of the particle. Considerable progress has been made in elucidating these relationships, which may lead to the development of predictable and robust single-beam acoustic handling devices.
© *2014 Acoustical Society of America*. [http://dx.doi.org/10.1121/1.4884758]

PACS number(s): 43.25.Qp, 43.25.Uv, 43.80.Ev, 43.20.Gp [ANN] Pages: 547–555

I. INTRODUCTION

Understanding the mechanisms through which acoustic beams push objects in the wave propagation direction or move objects laterally toward or away from the beam axis is relatively straightforward using the conventional radiation force theory. However, using a single gradientless symmetric acoustic beam to produce negative radiation forces (NRF) on a particle placed on the beam axis is more complex, and its underlying physics is not yet fully understood. In the case of a zero-order Bessel beam (ZOBB), for instance, numerical studies have shown that the radiation force on rigid/soft particles is always repulsive, whereas that for acoustically penetrable objects may become negative under specific conditions.[1–12] In the absence of gradient and absorption forces, this can only be interpreted to be due to the scattering forces and the structural properties of the object itself. Despite the recent works on the emergence of NRFs due to Bessel beams,[3–7] to the best knowledge of the author, the relation between the structural properties of the particles, e.g., mechanical properties and eigenfrequencies, and the emergence of NRFs on spheres due to an acoustic ZOBB has not been studied before. Development of a robust and predictable single-beam handling technique can lead to the development of advanced technologies for handling/sifting of micro-particles, based on their sizes or mechanical properties (e.g., white and red blood cells; see Fig. 1).

The application of Bessel beams of zero- and high-order (helicoidal) and focused beams for particle manipulation has been the subject of much theoretical and experimental studies in optics and more recently in acoustics.[1–13] Studies have shown that spherical particles placed on the axis of a Bessel beam may be attracted toward the source of the beam for appropriately selected beam parameters (shape and frequency) and particle properties (optical or mechanical).[1–13] Several theoretical studies have been carried out over the past few years to explore the feasibility of using ordinary (zeroth-order) and high-order Bessel beams for handling of on-axis objects with different mechanical properties.[3–12] The scattering of Bessel beams by liquid, solid elastics, and porous spheres have also been investigated in some recent papers.[10,11,14–16] Unlike high-order Bessel beams, an ordinary Bessel beam does not carry an orbital momentum and has no on-axis phase singularity, and therefore the emergence of NRFs using an ordinary Bessel beam, in a way, is even more intriguing.

As mentioned earlier, it can be readily shown that the axial radiation force due to a ZOBB on acoustically rigid/soft particles (i.e., admit no fields into its interior) is always repulsive, while that for drops, elastic, viscoelastic, and porous particles has been shown in recent investigations to be achievable over specific frequency bands.[3–12] It has been tried before to relate the emergence of such negative axial forces to the far-field characteristics of the object. For instance, for an optical Bessel beam, Chen *et al*. have shown that only if the radiation is emitted predominantly in the forward direction may a large backward recoil force then occur and give rise to NRFs on the object.[2] Likewise, in acoustics, Zhang and Marston illustrated some geometrical aspects of the momentum transport associated with negative radiation forces and showed that NRFs occur when the scattering into the backward hemisphere is suppressed relative to the scattering into the forward hemisphere.[6] Based on the derivation of acoustic radiation force developed by Zhang, and Marston,[6] the axial force on a lossless sphere is related to $\cos(\beta) - \langle w \rangle$, where $\langle w \rangle$ is the scattering asymmetry parameter and β is the conical angle of the beam [see Eq. (21) of Zhang and Marston[6]]. Therefore the necessary condition for the emergence of NRFs on a lossless spherical particle has been found to be $\langle w \rangle > \cos(\beta)$. The effect of particle's absorption has also been discussed.[6] Numerical analysis based on this condition shows that it can accurately predict the ka - β position of the NRF islands. In this study,

[a)]Author to whom correspondence should be addressed. Electronic mail: m.azarpeyvand@bristol.ac.uk

Redistribution subject to ASA license or copyright; see http://acousticalsociety.org/content/terms. Download to IP: 137.222.120.226 On: Wed, 06 Apr 2016 13:18:52

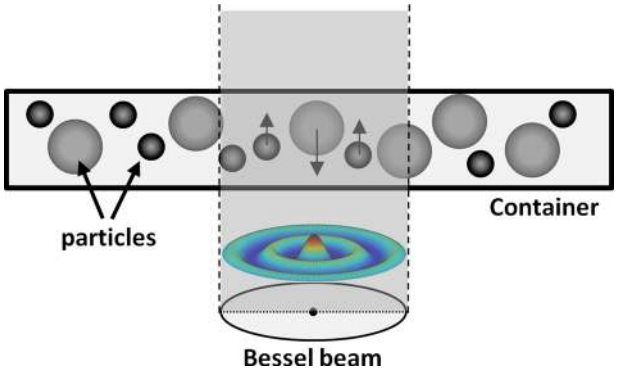

FIG. 1. (Color online) Interaction of a zero-order Bessel beam with uneven-sized particles in a container slab and production of attractive and repulsive forces.

however, we will show that in addition to the condition developed by Zhang and Marston,[6] one can also use the structural characteristics, namely mechanical properties and eigenfrequencies, of the particle to locate the NRF islands due to a ZOBB. In this study, we shall numerically investigate the emergence of NRFs for a wide range of materials, i.e., liquid and solid elastic, and will relate the emergence of such NRFs to the eigenfrequencies of the particle.

II. FORMULATION

In what follows, we shall consider the acoustic radiation force acting on an acoustically penetrable sphere (droplet and solid elastic), with radius a, placed on the axis of a ZOBB, in a lossless liquid medium with density and speed of sound of ρ_f, c_f, see Fig. 1. The velocity potential field of a symmetric incident sound beam can be expressed in cylindrical coordinates (R, z), in terms of a Bessel transform with respect to R and two Fourier transforms with respect to variables z, and t,[17]

$$\phi^{(inc)}(R,z,t) = \phi_0 \int_0^{\omega/c} \int_{-\infty}^{\infty} \mu J_0(\mu R)\, e^{i\gamma z - i\omega t} S(\mu,\omega) d\omega\, d\mu, \tag{1}$$

where ϕ_0 is the real-valued incident field amplitude constant, $\gamma = k\cos\beta$ and $\mu = k\sin\beta$ are, respectively, the longitudinal and transverse wavenumbers of the incident field, with $k = \omega/c_f$, $J_0(\cdot)$ is the Bessel function of order zero,[18] and $S(\mu,\omega)$ is the spectral function of the beam.[17] In the case of a ZOBB, the spectral function is given by, $S(\mu,\omega) = (1/\mu)\delta(\mu - k\sin\beta)\delta(\omega - \omega_0)$, which after substitution into the preceding integral representation of the incident field yields,

$$\phi^{(inc)}(R,z,\varphi) = \phi_0 J_0(\mu R)\, e^{i\gamma z - i\omega t}. \tag{2}$$

A closer inspection of the integral representation of the incident wave, Eq. (1), reveals that an axially symmetric Bessel beam is essentially the result of the superposition of plane-wave components the wave vectors of which lay on the surface of a cone having the propagation axis as its symmetry axis and an angle equal to β (conical angle).[17] Because acoustic radiation force on spherical objects is of interest, one first needs to rearrange the incident field expression, Eq. (2), in terms of spherical harmonic basis functions. Using the wave series expansion for cylindrical waves, see Eq. (82), page 413 of Stratton,[19] one can express the incident field in the spherical coordinate system (r, θ) as

$$\phi^{(inc)}(r,\theta) = \phi_0\, e^{-i\omega t} \sum_{n=0}^{\infty} i^n (2n+1) j_n(kr) \times P_n(\cos\beta) P_n(\cos\theta), \tag{3}$$

where j_n is a spherical Bessel function and P_n a Legendre function.[18] The interaction of the incident wave with an acoustically penetrable object, submerged in an inviscid fluid, results in the formation of a compressional sound field in the surrounding medium and an internal (transmitted) sound field. The form of the transmitted sound field depends on the mechanical characteristics of the particle (liquid, elastic, etc.), which will be dealt with later. The scattered sound field in the host medium can be readily expressed in spherical coordinate system as

$$\phi^{(sca)}(r,\theta) = \phi_0\, e^{-i\omega t} \sum_{n=0}^{\infty} i^n (2n+1) x_n h_n^{(1)}(kr) \times P_n(\cos\beta) P_n(\cos\theta), \tag{4}$$

where x_n are the partial wave scattering coefficients, and $h_n^{(1)}(\cdot) = j_n(\cdot) + iy_n(\cdot)$ denotes the Hankel function of the first order.[18]

The acoustic radiation force on a sphere can be calculated using $\mathbf{F} = \oint_A \mathbf{S}\cdot d\mathbf{A}$ where $\mathbf{S} = -\langle p\mathbf{I} - \rho_f \mathbf{vv}\rangle$ is the Brillouin radiation stress-tensor, and $p = \rho_f d\phi/dt$ and $\mathbf{v} = -\nabla\phi$ are the acoustic pressure and particle velocity in the surrounding fluid, respectively,[20–22] with $\phi = \mathrm{Re}(\phi^{(inc)} + \phi^{(sca)})$. In the preceding integral radiation force equation, $\langle\cdot\rangle$ denotes time average and the integration is performed over a fixed surface A around the scatterer. The time average of the acoustic radiation pressure can be obtained by integrating the Bernoulli equation, i.e., $\langle p\rangle = \langle \frac{1}{2}p^2/\rho_f c_f^2 - \frac{1}{2}\rho_f |\mathbf{v}|^2\rangle$, which then leads to[20–22]

$$\mathbf{F} = -\oint_A \left\{ \rho_f \langle \mathbf{vv}\rangle \cdot d\mathbf{A} - \frac{\rho_f}{2}\langle |\mathbf{v}|^2\rangle \cdot d\mathbf{A} + \frac{1}{2\rho_f c_f^2}\langle p\rangle^2 \cdot d\mathbf{A} \right\}. \tag{5}$$

The fact that the equation of a ZOBB is equivalent to the superposition of weighted plane-wave components, as seen in Eq. (3), allows us to find the exerted radiation force by using the general radiation force expression developed by Chen and Apfel[23] for any axisymmetric acoustic fields, although the case of ZOBB was not mentioned in their paper. The acoustic radiation force equation for ZOBB can also be found in other papers.[3,4] The experienced time-averaged acoustic radiation force on a sphere due to a ZOBB can then be written as $Y_p(ka,\beta) = -4(ka)^{-2}\sum_{n=0}^{\infty} Y_{p,n}$, where the nth modal contribution term $(Y_{p,n})$ are given by[3,4,23]

Redistribution subject to ASA license or copyright; see http://acousticalsociety.org/content/terms. Download to IP: 137.222.120.226 On: Wed, 06 Apr 2016 13:18:52

$$Y_{p,n} = (n+1)[\alpha_n + \alpha_{n+1} + 2(\alpha_n\alpha_{n+1} + \beta_n\beta_{n+1})] \times P_n(\cos\beta)P_{n+1}(\cos\beta), \quad (6)$$

where α_n and β_n are the real and imaginary parts of the scattering coefficients, x_n. Equation (6) somewhat reveals the connection of $Y_{p,n}$ to both the nth and the $(n+1)$th partial wave components due to the presence of x_{n+1} scattering coefficient terms and the last Legendre term of the nonparaxiality parameter $[P_n(\cos\beta)P_{n+1}(\cos\beta)]$. The effects of this interconnection will be discussed later for the prediction of the effective conical ranges over which NRFs may occur. It is worth mentioning that this interconnection between different modal radiation force components disappears at the complex-valued eigenfrequencies of the system. This important property of radiation force components will be used later in Sec. III C for finding the effective conical angle range of each NRF island.

The mechanical and structural properties of particles can be studied using their farfield form-function spectra. The acoustic form-function for the scattering of a ZOBB by an ideal sphere in an ideal inviscid fluid can be defined in terms of the far-field pressure (p_s), as $F(ka,\ \theta) = (2r/a)e^{-ikr}\ p_s(ka,\ \theta,\ \varphi)$, where upon using the high-frequency asymptotic form of the spherical Hankel function, i.e., $i^p h_p(kr) \sim (1/ikr)e^{ikr}(kr \to \infty)$, reduces to $F(ka,\theta) = -2(ka)^{-1}\sum_{n=0}^{\infty} F_n$, where the partial-wave form-function components F_n are given by

$$F_n = i(2n+1)(\alpha_n + i\beta_n)P_n(\cos\beta)P_n(\cos\theta). \quad (7)$$

For the two scenarios considered in this paper, namely liquid drops and solid elastic spheres in a fluid medium, the partial wave scattering coefficients can be found from

$$x_n = -\frac{\mathfrak{Q}_n j_n(ka) - j_n'(ka)}{\mathfrak{Q}_n h_n(ka) - h_n'(ka)}, \quad (8)$$

where $\mathfrak{Q}_n$ for a submerged liquid drop with density of ρ_d and speed of sound c_d, is given by

$$\mathfrak{Q}_n = \frac{1}{\gamma_d}\frac{j_n'(X_d)}{j_n(X_d)}, \quad (9)$$

where $X_d = ka/\bar{c}_d$, $\bar{c}_d = c_d/c_f$, $\bar{\rho}_d = \rho_d/\rho_f$, and $\gamma_d = \bar{c}_d\bar{\rho}_d$ is the drop-to-host acoustic impedance ratio. Also in the case of a submerged elastic sphere of density ρ_s, and Lame's constants λ and μ, $\mathfrak{Q}_n$ is given by[24,27]

$$\mathfrak{Q}_n = \frac{1}{2ka}\frac{X_T^2}{\bar{\rho}_s}\frac{\dfrac{X_L j_n'(X_L)}{X_L j_n'(X_L) - j_n(X_L)} - \dfrac{2n(n+1)j_n(X_T)}{(n+2)(n-1)j_n(X_T) + X_T^2 j_n''(X_T)}}{X_L^2\dfrac{(0.5X_T^2/X_L^2 - 1)j_n(X_L) - j_n''(X_L)}{X_L j_n'(X_L) - j_n(X_L)} - \dfrac{2n(n+1)\left[j_n(X_T) - X_T j_n'(X_T)\right]}{(n+2)(n-1)j_n(X_T) + X_T^2 j_n''(X_T)}}, \quad (10)$$

where $X_{L,T} = ka/\bar{c}_{L,T}$, $\bar{\rho}_s = \rho_s/\rho_f$ is the density ratio, $\bar{c}_{L,T} = c_{L,T}/c_f$ are the longitudinal and transverse speed of sound ratios, with $c_L = \sqrt{(\lambda+2\mu)/\rho_s}$ the longitudinal wave speed and $c_T = \sqrt{\mu/\rho_s}$ the transverse wave speed. The ratio of the speeds of transverse and compressional waves can be defined using Poisson's ratio (ν) through $c_T/c_L = [2 + 2\nu/(1-2\nu)]^{-1/2}$.

III. NUMERICAL RESULTS AND DISCUSSIONS

The emergence of negative axial radiation forces due to diffraction-free acoustic beams, like ZOBBs, is an interesting topic and has many practical implications. However, what is perhaps more important than the emergence of NRFs itself, is the underlying physics of such phenomenon and the issue of predictability of such negative axial radiation forces, i.e., predicting the ka - β range over which the axial force reveres. Because ZOBBs do not produce NRFs on acoustically rigid/soft particles (i.e., perfectly reflective) and the axial force due to beam's gradient is zero, the answer to this question must be sought in the dynamic characteristics of particles. A set of MATLAB codes have been developed to calculate the acoustic radiation force and form-function for liquid and solid elastic spheres. The radiation force and form-function results have been validated against the available results for plane progressive wave and ZOBB.[3–5,25] The computations have been performed on a dual-core computer with truncation constant of $N_{max} = 50$ to assure the convergence of the simulations in the chosen ka-bandwidth. To properly detect the NRFs and also the eigenfrequencies of the particle, small wavenumber increments have been used. The NRF survey simulations, i.e., Figs. 3(a) and 4, are performed with a wavenumber increment of $\Delta ka = 10^{-2}$, and the results in other figures are obtained using a wavenumber increment of $\Delta ka = 10^{-3}$.

The dynamics of an acoustically penetrable object cannot be fully addressed without studying the complex-valued eigenfrequencies of the system. A conventional way for examining the complex eigenfrequencies of an acoustic scattering problem is to plot the form-function modulus, here $|F(ka, \theta = \pi)|$, over the two-dimensional complex plane of ka.[25] The complex eigenfrequencies can be defined by $X_{n,l} = \alpha_{n,l} - \frac{1}{2}i\Gamma_{n,l}$, where $n = 0,1,2,\ldots$ specifies the fundamental frequency and $l = 1,2,3,\ldots$, identifies the overtones associated with the fundamental mode of the vibration the members of which appear in all the partial waves, shifting to higher frequencies from one partial wave to the next.[24–30] The quantity $\Gamma_{n,l}$ shows the distance of the resonance to the real axis, and $(\Gamma_{n,l})^{-1}$ is a measure of the lifetime of the

Redistribution subject to ASA license or copyright; see http://acousticalsociety.org/content/terms. Download to IP: 137.222.120.226 On: Wed, 06 Apr 2016 13:18:52

resonance. More detailed discussions about the above-mentioned vibrational modes and their lifetime can be found in the literature.[24–30]

In the case of solid elastic materials, these eigenfrequencies (poles), generally, fall into two main categories depending on whether their phase velocities lie close to the elastic bulk wave speeds in the solid, i.e., Rayleigh ($l=1$) and Whispering-gallery type modes $l=2, 3,\ldots$, or to the acoustic wave speed in the fluid, i.e., Franz-type creeping modes. The modes in the first category are due to the resonances of internal waves and usually close to the real frequency axis (i.e., slightly attenuated), and therefore their effects are more visible in form-function spectra, whereas the Franz creeping modes spin the surface of the sphere's circumference with successively increasing integer numbers of wavelength and are highly attenuated and thus their effects are hard to detect. In what follows, the Rayleigh and Whispering-gallery modes of nth vibrational mode and lth order for solid elastic objects will be denoted by R_{nl}, and the Franz modes by F_{nl}. The poles lie only in the fourth quadrant $\mathrm{Re}(ka)>0$, and $\mathrm{Im}(ka)<0$. It is important to note that in the case of liquid spheres, particles do not support Rayleigh modes, and all the poles near the $\mathrm{Im}(ka)=0$ axis are the Whispering-gallery modes. To avoid confusion, however, we shall use the "R" notation to denote both the Rayleigh and Whispering-gallery modes for both liquid and solid elastic spheres. An example is provided in Fig. 2 for a droplet in water with $\bar{\rho}_d=1.26$, and $\bar{c}_d=1.28$, for the first four vibrational modes $n=0$–3 (poles shown as dark regions). The Whispering-gallery modes are those closer to the real axis (marked by R), while the first round of the Franz creeping modes (marked by F), are further down, with much greater imaginary part ($\Gamma_{n,l}$).

A. NRFs on liquid drops

The axial radiation force and complex eigenfrequencies calculations have been performed for a large number of liquid-liquid cases within the density ratio range of $0.3<\bar{\rho}_d<2$, and speed of sound ratio range of $0.4<\bar{c}_d<1.4$. The host medium in these simulations is water ($\rho_f=1000\,\mathrm{kg\ m^3}$, $c_f=1480\,\mathrm{ms^{-1}}$). Figure 3(a) provides results for the feasibility of producing NRFs on liquid drops using ZOBB based on their mechanical properties, i.e., $\bar{c}_d$ and $\bar{\rho}_d$. The NRF survey has been performed over $0.01<ka<15$ (with wavenumber increment of $\Delta ka=0.01$) and $0°<\beta<90°$ and the colored ρ_d/ρ_f-c_d/c_f area in Fig. 3(a) shows where negative radiation forces can be achieved. Regarding the possibility of the emergence of NRFs on liquid cases of practical importance ($0<\bar{\rho}_d<3$), numerical analysis has shown that NRFs due to a ZOBB generally occur if $\bar{c}_d<1.46$, except for gas-liquid cases where $\bar{\rho}_d\approx 0$ [Fig. 3(a)]. Concerning the number of the NRF islands over $0.01<ka<15$ for liquid drops, the speed of sound ratio $\bar{c}_d=1$ is found to be a critical value, above which ($1<\bar{c}_d<1.46$) there exists only one dominant NRF island, e.g., a glycerol-like drop in water ($\bar{c}_d=1.28$, $\bar{\rho}_d=1.26$) (ignoring solubility), see Fig. 3(b1), and below which multiple NRF islands appear, e.g., chloroform drop in water ($\bar{c}_d=0.67$, $\bar{\rho}_d=1.49$), see Fig. 3(b2). It must be mentioned that the materials mentioned here are chosen solely based on their speed of sound and density ratios to provide a comprehensive numerical study and the effects of their other mechanical and chemical properties such as solubility or reactivity are not considered.

It is also important to note that in addition to the typical NRF islands, similar to those shown in Fig. 3(b) (and Fig. 7 of Marston[3]), there is also a category of very low amplitude NRF islands at low frequencies ($ka<0.5$), reported by Marston.[6] Using a low frequency approximation, i.e., dominated by the monopole and dipole terms, Marston showed that the exerted radiation force due to a ZOBB can be expressed as[3]

$$Y_{P,LF}=\left(\frac{2ka}{1+2\bar{\rho}_d}\right)^2\left[\mathrm{G}^2+\frac{2}{9}(1-\bar{\rho}_d)^2P_2(\cos\beta)\right]\cos\beta, \tag{11}$$

where $\mathrm{G}=\bar{\rho}_d-\left[(1+2\bar{\rho}_d)/3\bar{\rho}_d\right]\bar{c}_d^2$. Because $\cos\beta$ is positive over $0°<\beta<90°$, for Y_p to be negative, the term in the square brackets must be negative. It can be readily shown, after some algebra, that the latter condition is equivalent to $\cos\beta<\sqrt{\left[1-9\mathrm{G}^2/(1-\bar{\rho}_d)^2\right]/3}$. In a limiting case, when $\mathrm{G}=0$ [shown in Fig. 3(a) by dashed line], the latter condition reduces to $\cos\beta<\sqrt{1/3}$, i.e., $54.73°<\beta<90°$, as per Marston.[3] The region over which $Y_{P,LF}$, Eq. (11), is negative is also shown in Fig. 3(a). Although the negative $Y_{P,LF}$ (marked with $Y_{P,LF}^-$) and the negative $Y_{p,n}$ regions (marked with Y_P^-) overlap over some $\bar{\rho}_d$ - $\bar{c}_d$ areas, numerical inspections have shown that the low frequency NRFs are of very small amplitude and lead to much larger NRFs at higher frequencies. An example of such a case was presented and discussed by Marston.[3]

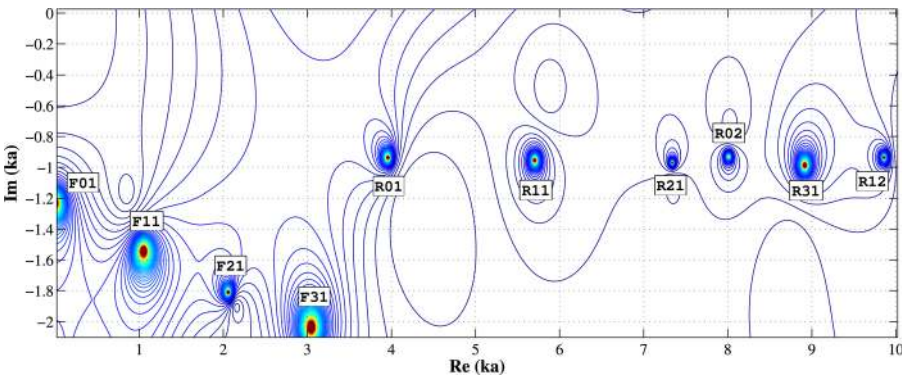

FIG. 2. (Color online) Complex-valued eigenfrequencies for scattering by a droplet immersed in water sphere in water with $\rho_d/\rho_f=1.26$, and $c_d/c_f=1.28$ for the first four modes ($n=0$–3). The Whispering-gallery modes are shown by "R" and Franz modes by "F."

Redistribution subject to ASA license or copyright; see http://acousticalsociety.org/content/terms. Download to IP: 137.222.120.226 On: Wed, 06 Apr 2016 13:18:52

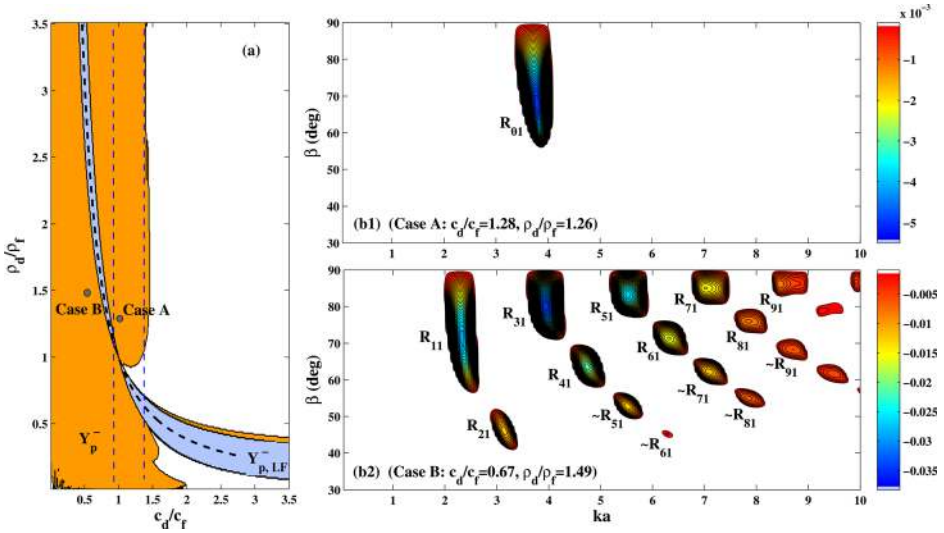

FIG. 3. (Color online) (a) Diagram for the possibility of the emergence of negative radiation forces on liquid droplets with different density and speed of sound ratios over $0.01 < ka \leq 15$ and $0° < \beta < 90°$. The outer colored region (Y_P^-) corresponds to when a ZOBB can produce NRF over $0.01 < ka \leq 15$, and the inner colored region corresponds to the low frequency NRFs ($Y_{P,LF}^-$), given by Eq. (11). The $G = 0$ line is also shown as dashed line. (b1) NRF islands for a drop with $\bar{c}_d = 1.28$, $\bar{\rho}_d = 1.26$ (glycerollike, ignoring the solubility); (b2) NRF islands for a drop with $\bar{c}_d = 0.67$, $\bar{\rho}_d = 1.49$ in water (like chloroform) and the corresponding eigenfrequencies.

Studying the partial-wave radiation force contributions ($Y_{p,n}$), in ka - β contour plot format, and complex eigenfrequency contours at each mode (n) using the form-function components (F_n), Eq. (7), enables us to track the advent of each NRF island and relate it to the dynamics of the object. The comparison of the NRF results (modal and total) and the corresponding complex eigenfrequencies for droplets with speed of sound ratio within the range of $1 < \bar{c}_d < 1.46$ has led to the conclusion that the only dominant NRF island, for instance, a glycerol-like drop in water (ignoring solubility), occurs at the first eigenfrequency, R_{01}, see for example Figs. 2 and 3b1. As we slowly decrease the speed of sound ratio toward the critical value $\bar{c}_d = 1$, the size and amplitude of the R_{01} island progressively decreases and will completely disappear within the range of $0.9 < \bar{c}_d < 1.0$. But, instead, some new NRF islands emerge at higher frequencies (relative to $\alpha_{0,1}$). These new islands, which appear at high conical angles, are found to be caused by the odd-numbered poles and their frequencies coincide with the R_{n1} ($n = 1, 3, 5,\ldots$) frequencies. For droplets with lower speed of sound ratios, $0.4 < \bar{c}_d < 0.9$, a second row of NRF islands will also occur at the even-numbered poles R_{n1} ($n = 2, 4, 6,\ldots$), at smaller conical angles (marked with $\sim R_{n1}$), see Fig. 3(b2). Thus for a drop with given mechanical properties ($\bar{c}_d$ and $\bar{\rho}_d$), one can easily find the exact ka position of the NRF islands using the eigenfrequencies of the particle. It is also important to note that the condition developed by Zhang and Marston,[6] i.e., $\langle w \rangle > \cos(\beta)$, where $\langle w \rangle = Y_1/Q_{\text{sca}}$, and in the case of ZOBBs, Y_1 and Q_{sca} are given by

$$Y_1 = \left(\frac{2}{ka}\right)^2 \sum_{n=0}^{\infty} \left[2(\alpha_n \alpha_{n+1} + \beta_n \beta_{n+1})\right](n+1) \times P_n(\cos\beta) P_{n+1}(\cos\beta), \tag{12a}$$

$$Q_{sca} = \left(\frac{2}{ka}\right)^2 \sum_{n=0} \left(|x_n|^2\right)(2n+1)[P_n(\cos\beta)]^2, \tag{12b}$$

can also accurately predict the ka - β location of the NRF islands, but it requires numerical calculation of the radiation force component $\langle w \rangle$. However, the eigenfrequency-based condition developed here shows that the advent of NRFs is related to the eigenfrequencies of the system and that the ka location of the NRF can be predicted without calculating the radiation force.

Finally, the ka range of different NRF islands have also been studied, and it has been observed that they depend on the width of the corresponding resonance ($\Gamma_{n,l}$), i.e., inversely related to the decay times (ringing) of the excited resonance, given by $\Delta t_{n,l} = a/(c_f \Gamma_{n,l})$. It is worth mentioning here that there is usually a mismatch between the real-valued resonance frequencies (*in vacuo*) obtained from form-function spectra and the complex-valued singularities obtained from complex-ka plane (under fluid loading). The issue of the dependence of distance of the complex singularity from the real axis $\left(\frac{1}{2}\Gamma_{n,l}\right)$ on the ratio of fluid to solid density has been investigated by several authors.[29,31] Our numerical assessment for fluids of practical interest has shown that this mismatch can be up to about $0.1\alpha_{n,l}$, while that for solid elastic spheres is much less.

B. NRFs on elastic spheres

In this section, we shall investigate the physical mechanisms of the emergence of NRFs on solid elastic spheres using ZOBBs. To understand the underlying mechanism, $ka - \beta$ NRF islands and eigenfrequencies have been calculated for more than 25 solid elastic materials with different densities, bulk, and rigidity moduli. In these simulations, the host medium is water ($\rho_f = 997\,\text{kg/m}^3$ and $c_f = 1484\,\text{m/s}$). Figure 4 provides results for the feasibility of producing NRFs using ZOBB based on their mechanical properties, i.e., $\bar{c}_L$, $\bar{c}_T$, and $\bar{\rho}_s$. The NRF survey is performed over $0.01 < ka < 15$ (with wavenumber increment of $\Delta ka = 0.01$) and $0° < \beta < 90°$. For materials with Poisson's ratio of $\nu \approx 0$, i.e., little lateral expansion when compressed, the transverse-to-longitudinal wave speeds ratio is maximum $\bar{c}_T/\bar{c}_L = 0.707$, while for almost incompressible materials ($\nu \approx 0.5$), the shear wave speed tends to zero. Regarding the possibility of the emergence of NRFs on solid spheres with density ratio of $\bar{\rho}_s > 2$, our numerical investigations have shown that the emergence and the number of the NRF islands depend

Redistribution subject to ASA license or copyright; see http://acousticalsociety.org/content/terms. Download to IP: 137.222.120.226 On: Wed, 06 Apr 2016 13:18:52

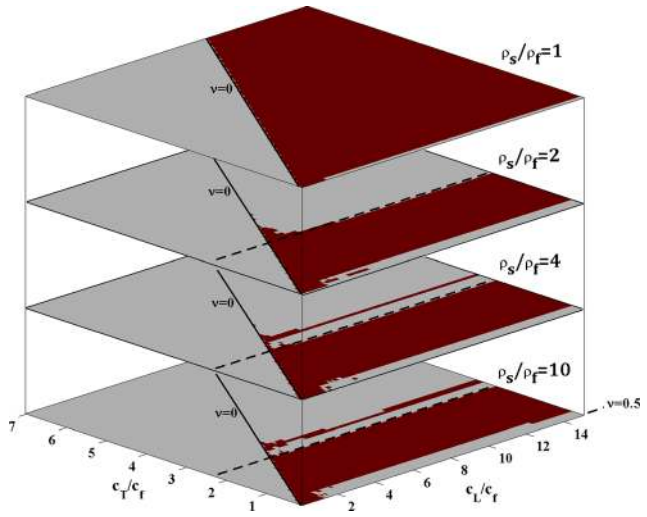

FIG. 4. (Color online) Diagram showing the possibility of the emergence of negative radiation forces on solid elastic particles, at different density and speed ratios ($\bar{\rho}_s$, $\bar{c}_{L,T}$). The dark regions correspond to when a ZOBB can produce negative radiation force. The possibility of emergence negative radiation forces is explored over $0.01 < ka \leq 15$.

primarily on the shear wave speed ratio (ξ_T) and have led to the $0.35 < \bar{c}_T < 2.2$ criterion (see Fig. 4), which can also be expressed as $0.12\bar{\rho}_s < \mu/K < 4.84\bar{\rho}_s$, where K is the modulus of bulk elasticity of the host fluid. It has to be mentioned that for materials with $\bar{c}_T$ close to the lower limit (such as *polymers*) or upper limit (such as *beryllium, stiff silica,* and *molybdenum*) of the preceding condition, NRF islands may only occur over very narrow *ka* ranges, which may be impractical to use. For most polymers of practical use, with density ratio range of $0.7 < \bar{\rho}_s < 1.3$, relative to water, such as nylon, polyethylene, NRFs occurs over multiple narrow-*ka* islands, with large β ranges. The scattering of ZOBB by a poly(methylmethacrylate) (PMMA) sphere and the emergence of NRF islands have been studied by Marston.[4,15] For materials with $\bar{c}_T > 2.2$, there are no proper NRF islands or they occur over very narrow frequency bands, such as beryllium, stiff silica, and molybdenum.

As mentioned earlier, materials of almost $\nu = 0.5$ (nearly incompressible) have negligible shear wave velocity and large c_L/c_T as a result. This implies that there is only a compressional wave within the particle, similar to an ideal liquid drop with $\rho_d = \rho_s$ and $c_d = c_L$. Therefore the NRF islands pattern of such materials will be very similar to the equivalent liquid case. This also implies that for such materials one can find the $\bar{c}_L$ - $\bar{\rho}_s$ condition for the emergence of NRFs using Fig. 3(a). The discussion provided in Sec. III. A regarding the low frequency NRF and the $G = 0$ locus [see Eq. (11)] can also be used for the determination of the $\bar{c}_L - \bar{\rho}_s$ areas for such materials.

In the rest of this section, discussions will be provided based on $\bar{c}_T$ regions defined earlier. As mentioned earlier, the inspection of the resonances of the particles can help us relate the NRFs to the structural characteristics of the particle and predict the NRF frequencies. To make the discussion easier to follow, the *ka* - β NRF islands for eight elastic materials with different mechanical properties are provided in Fig. 5. As seen in Fig. 5, for elastic spheres with $2 < \bar{c}_T < 2.2$, such as *aluminum, steel,* and *titanium,* there exists only one dominant NRF island within the considered frequency band. The inspection of the modal radiation force contributions ($Y_{p,n}$), and the corresponding eigenfrequencies of the particle ($X_{n,l}$) has shown that this dominant NRF island occurs at the Rayleigh mode R_{21} (spheroidal mode) of the particle. The backscattered form-function results for these materials show a significant dip over the NRF frequencies, see Fig. 6 (the aluminum spectrum), as per Marston.[3,6] The spheroidal R_{21} mode has the lowest frequency for a free elastic sphere and corresponds to the prolate-to-oblate spheroidal motion of the particle. The formation of a strong dip in the backscattering form-function spectrum at R_{21} is a well-studied matter.[26] Although the suppression of back-scattered sound field for solid elastic spheres with $2 < \bar{c}_T < 2.2$, such as aluminum, over the NRF frequency band has been mentioned before,[3,8] the relation between the NRF island and the R_{21} mode has not been discussed.

For relatively soft metal spheres with $1.1 < \bar{c}_T < 2$, such as *copper, platinum, tin, brass,* and *silver,* multiple NRF islands can be found over the considered *ka* - β domain, see Fig. 5. The numerical evaluation of the exerted radiation force has shown that as the transverse speed of sound ratio decreases below about $\bar{c}_T = 2$, the R_{21}-NRF islands gradually disappear and instead some new NRF islands will emerge, excited by the higher-order Rayleigh modes. The lowest frequency island for such materials is due to the R_{31} Rayleigh mode with the higher-order Rayleigh mode NRFs appearing at higher frequencies, Fig. 5. The results for the cases considered in this study have also shown that the Whispering-gallery modes, such as R_{32} and R_{42}, may also cause NRFs at frequencies greater than that of R_{51}. It is important to note that the high-order Rayleigh or Whispering-gallery modes may not cause a noticeable minimum in the backscattering form-function spectrum due to the large conical angle of the ZOBB. Some examples are provided in Fig. 6 for the form-function of a submerged copper and zinc spheres illuminated by ZOBB with $\beta = 85°$ and the frequency bands that NRFs occur are shown by thick lines. The issue of occurrence of form-function minima at resonance frequencies has been discussed in Williams and Marston,[28] and it has been shown that the resonances could cause either peaks or depressions in the backscattering depending on whether the specular reflection is in phase or out of phase with the guided-wave contribution. In the case of scattering of ZOBBs, it has been shown by Martson[15] that the backscattering may be reduced or increased depending on properties of the resonance and of the specular contribution and that the conical angle can be chosen such that the excitation of a given guided wave is suppressed.

Last, as demonstrated earlier for the liquid sphere cases, the *ka* ranges of the NRF islands for elastic spheres have also been found to be related to the width of the excited resonance ($\Gamma_{n,l}$). As an example, the *ka* ranges of the R_{21}-NRF for glass, aluminum, and iron spheres are found to be, respectively, $4.84 < ka < 5.54$ ($\Delta ka = 0.7$), $4.72 < ka < 5.22$ ($\Delta ka = 0.5$), and $5.47 < ka < 5.68$ ($\Delta ka = 0.21$) (see Fig. 5),

Redistribution subject to ASA license or copyright; see http://acousticalsociety.org/content/terms. Download to IP: 137.222.120.226 On: Wed, 06 Apr 2016 13:18:52

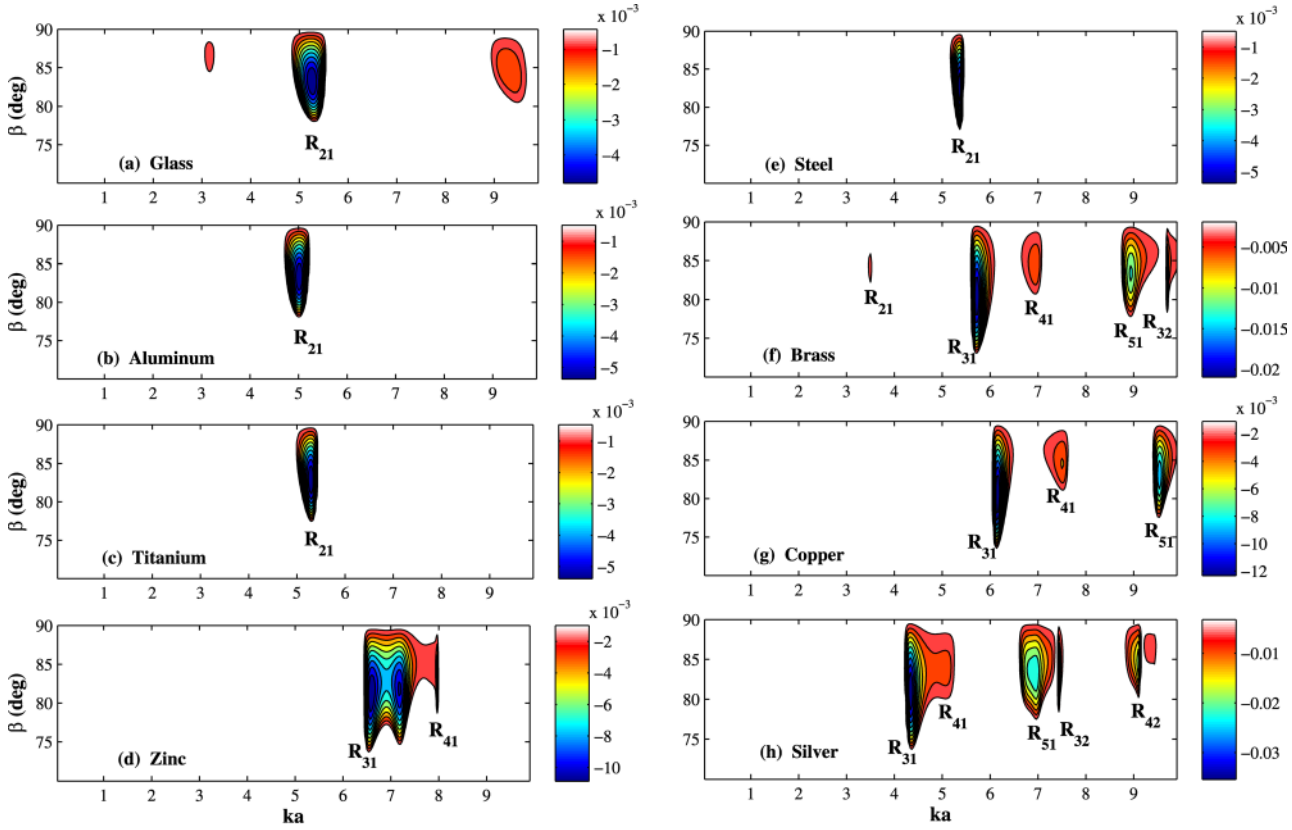

FIG. 5. (Color online) Negative radiation force islands for elastic spheres in water. (a) Glass [$\rho_s = 2.32\,\mathrm{g/cm^3}$, $c_L = 5640\,\mathrm{m/s}$, $c_T = 3280\,\mathrm{m/s}$], (b) aluminum [2.7, 6420, 3040], (c) titanium [4.5, 6070, 3125], (d) zinc [7.1, 4210, 2440], (e) steel [7.9, 5790, 3100], (f) brass [8.6, 4700, 2110], (g) copper [8.93, 5010, 2270], and (h) silver [10.4, 3650, 1610].

and their resonance widths are, respectively, $\Gamma_{2,1} \approx 0.98$, 0.78, and 0.27. Also, the Rayleigh NRFs have been found to have larger *ka* ranges than the Whispering-gallery NRFs; this is consistent with the prior studies concerning the width of the Rayleigh and Whispering-gallery resonances.[27] A detailed discussion on the issue of resonance width and its dependence on the ratio of fluid to solid density can be found in Marston[29] and Norris.[31]

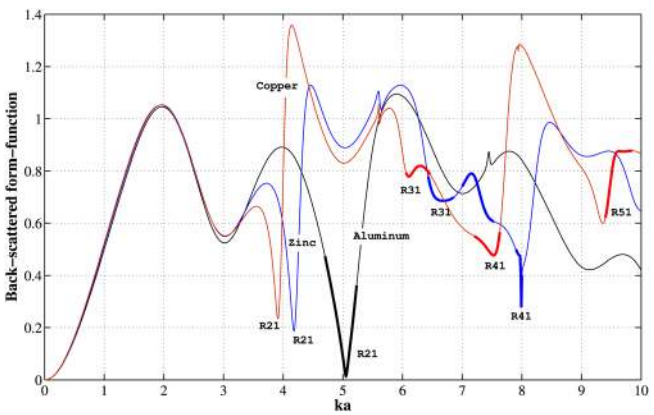

FIG. 6. (Color online) Back-scattering form-function for aluminum [2.7 gr/cm^3, 6420 m/s, 3040 m/s], zinc [7.1, 4210, 2440] and copper [8.93, 5010, 2270] spheres suspended in water illuminated by a ZOBB with $\beta = 85°$. The thick lines show where the radiation force becomes negative.

C. Conical angle range

The second step for the development of a ZOBB tractor is to find the effective conical angle range ($\angle\beta$). Because we have established that in the case of ZOBBs, the emergence of NRFs depends on the location of the eigenfrequencies of the system, finding the conical angle range becomes somewhat easier. It can be readily shown that at a particular complex eigenfrequency of the system, say the eigenfrequency for a given (n, l), the nth partial wave scattering coefficient is much larger than other scattering coefficients, i.e., $|x_n| \gg |x_m|$, where $m = 0, 1, 2, \ldots$, and $m \neq n$. As seen in Eq. (6) and also the Y_1 radiation force component in Eq. (12), the nth partial wave scattering coefficient x_n, enters into two modal radiation force components, i.e., $Y_{p,n-1}$, and $Y_{p,n}$.

Because, at the nth eigenfrequency $|x_n| \gg |x_m|$ ($m \neq n$), to find the effective conical angle range ($\angle\beta$), it is sufficient to only focus on the $Y_{p,n-1}$, and $Y_{p,n}$ radiation force components rather than the whole radiation force equation, Y_p. By doing so, one can establish a condition for $\angle\beta$ based on the nonparaxiality parameters, $P_q(\cos\beta)P_{q+1}(\cos\beta)$, involved in $Y_{p,n-1}$, and $Y_{p,n}$. Figure 7 shows the behavior of the nonparaxiality parameter, $P_n(\cos\beta)P_{n+1}(\cos\beta)$ over $\beta = 0°$–$90°$ for $n = 0$–6. The method explained in the preceding text has been used for all the cases considered in Secs. III A and III B, and the outcomes are listed in the following text.

Redistribution subject to ASA license or copyright; see http://acousticalsociety.org/content/terms. Download to IP: 137.222.120.226 On: Wed, 06 Apr 2016 13:18:52

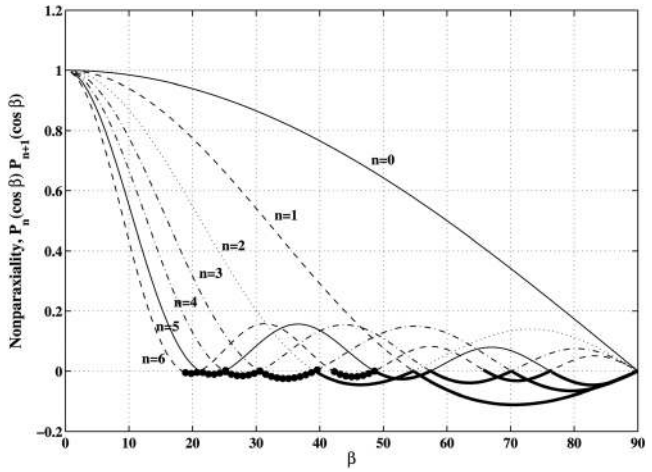

FIG. 7. The nonparaxiality term in the radiation force, $P_n(\cos\beta)P_{n+1}(\cos\beta)$, for different modes. The last negative nonparaxiality regions are shown by think lines and the second to the last by circles.

(1) The conical angle range ($\angle\beta$) for odd-numbered islands $R_{2t\text{-}1,1}$ ($t=1,\ 2,\ldots$) can be determined from $P_{2t\text{-}1}(\cos\beta)P_{2t}(\cos\beta)<0$. The negative nonparaxiality regions are shown by thick lines in Fig. 7. According to this criterion, the $\angle\beta$ for R_{11}, R_{31}, and R_{51} are roughly [54°–90°], [70°–90°], and [76°–90°], respectively; this agrees well with the results in Figs. 3b2 and 5. The conical angle range for the secondary odd-numbered islands ($\sim R_{2t\text{-}1,1}$), appeared in the case of drops with $\bar{c}_d<1$, are given by the second to the last solution range of $\angle\beta$ condition, shown in Fig. 7 by circles.

(2) The conical angle range ($\angle\beta$) for even-numbered islands R_{2t} ($t=0,\ 1,\ 2,\ldots$) for solid elastic cases and drops with $\bar{c}_d>1$ (i.e., one dominant R_{01} island) are found to be determined by $P_{2t+1}(\cos\beta)P_{2t+2}(\cos\beta)<0$, due to the interaction of the attractive $Y_{p,2t+1}$ and repulsive $Y_{p,2t}$ radiation force components. As the comparison of Figs. 2 and 5 and 7 suggests $\angle\beta$ for R_{01}, R_{21}, and R_{41} are roughly [54°–90°], [70°–90°], and [76°–90°], which are consistent with the preceding condition. The even-numbered islands for liquid cases with $\bar{c}_d<1$, on the other hand, are found to be given by the $P_{2t}(\cos\beta)P_{2t+1}(\cos\beta)<0$ condition, see for example the comparison of R_{21} and R_{41} in Fig. 3-b2 and the nonparaxiality results in Fig. 7 for $n=2$ and 4. For solid elastic cases, the agreement is usually 1° or 2° off due to the modal interferences.

The preceding two eigenfrequency-based conditions for $\angle\beta$ have also been checked against the results available in other studies and have shown excellent agreement.

As mentioned by Marston,[6] and also reviewed in the preceding text, there is also a category of very low frequency NRFs the conical angle range ($\angle\beta$) of which must also be considered. In the case of liquid drops, this type of low frequency NRFs lead to a larger NRF island (R_{01} or R_{11}) at higher frequencies (see for example Fig. 8 of Marston[3]), and its conical angle range is also the same as the associated higher frequency NRF island, which is given by $P_1(\cos\beta)P_2(\cos\beta)<0$, i.e., $\angle\beta=[54.73°–90°]$. Also the preceding discussion shows that if one knows the eigenfrequencies of the particle under consideration, the condition developed by Zhang and Marston,[6] $\langle w\rangle>\cos(\beta)$, at the nth mode, can be further simplified to only include the significant components, as

$$Y_1\approx\left(\frac{2}{ka}\right)^2\sum_{q=n-1}^{n}2(q+1)\mathrm{Re}\left(x_q x_{q+1}^*\right)\times P_q(\cos\beta)P_{q+1}(\cos\beta), \tag{13a}$$

$$Q_{sca}\approx\left(\frac{2}{ka}\right)^2|x_n|^2(2n+1)[P_n(\cos\beta)]^2. \tag{13b}$$

Finally, equating the β derivate of the angular part of the modal radiation force components to zero, one can show that the magnitude of the realized NFR within the R_{n1} island peaks where $P_{n+1}(\cos\beta_{max})+P_n(\cos\beta_{max})=0$. Using the eigenfrequency-based method proposed in Secs. III, one can find the ka location of the NRF islands, their non-paraxiality range ($\angle\beta$) and also the optimum conical angle β_{max}. This will help to tune the beam to exert an attractive force on a particle, with known mechanical and structural properties without a need to calculate the acoustic radiation force.

IV. CONCLUSION

The problem of emergence of negative axial radiation forces on acoustically penetrable spheres due to a zero-order Bessel beam has been revisited from a structural dynamic perspective. Significant progress has been made in understanding of the feasibility, predictability, and underlying physics of such phenomena. Our investigations have shown that the most dominant negative radiation force islands in the case of liquid drops are due to the R_{01} or R_{11} eigenfrequencies, while that for solid elastic spheres are caused by the R_{21} and R_{31} resonances. A new method has also been proposed for the prediction of the beam nonparaxiality range over which the axial radiation force reverses. The approach proposed in this study can also be used to understand the emergence of negative radiation forces on shells with different mechanical properties.

ACKNOWLEDGMENT

The author gratefully acknowledges the financial support from the Royal Academy of Engineering.

[1]A. Novitsky, C.-W. Qiu, and H. Wang, "Single gradientless light beam drags particles as treactor beams," Phys. Rev. Lett. **107**, 203601 (2011).
[2]J. Chen, J. Ng, Z. Lin, and C. T. Chan, "Optical pulling force," Nat. Photon. **5**, 531–534 (2011).
[3]P. L. Marston, "Axial radiation force of a Bessel beam on a sphere and direction reversal of the force," J. Acoust. Soc. Am. **120**, 3518–3524 (2006).
[4]P. L. Marston, "Negative axial radiation force on solid spheres and shells in a Bessel beam (L)," J. Acoust. Soc. Am. **122**, 3162–3165 (2007).
[5]P. L. Marston, "Radiation force of a helicoidal Bessel beam on a sphere," J. Acoust. Soc. Am. **125**, 3539–3547 (2009).
[6]L. Zhang and P. L. Marston, "Geometrical interpretation of negative radiation forces of acoustical Bessel beams on spheres," Phys. Rev. E **84**, 035601 (2011).

Redistribution subject to ASA license or copyright; see http://acousticalsociety.org/content/terms. Download to IP: 137.222.120.226 On: Wed, 06 Apr 2016 13:18:52

[7]L. Zhang and P. L. Marston, "Axial radiation force exerted by general non-diffracting beams," J. Acoust. Soc. Am. **131**, EL329–EL335 (2012).
[8]F. G. Mitri, "Negative axial radiation force on a fluid and elastic spheres illuminated by a high-order Bessel beam of progressive waves," J. Phys. A Math. Theor. **42**, 245202 (2009).
[9]F. G. Mitri, "Langevin acoustic radiation force of a high order Bessel beam on a rigid sphere," IEEE Trans. Ultrason. Ferroelectr. Freq. Control **56**, 1059–1064 (2009).
[10]M. Azarpeyvand, "Acoustic radiation force of a Bessel beam on a porous sphere," J. Acoust. Soc. Am. **131**, 4337–4348 (2012).
[11]M. Azarpeyvand and M. Azarpeyvand, "Application of acoustic Bessel beams for handling of hollow porous spheres," Ultrasound Med. Biol. **40**, 422–433 (2014).
[12]M. Azarpeyvand, M. A. Alibakhshi, and R. Self, "Effects of multi-scattering on the performance of a single-beam acoustic manipulation device" IEEE Trans. Ultrason. Ferroelectr. Freq. Control **59**, 1741–1749 (2012).
[13]M. Azarpeyvand and M. Azarpeyvand, "Acoustic radiation force on a rigid cylinder in a focused Gaussian beam," J. Sound Vib. **332**, 2338–2349 (2013).
[14]P. L. Marston, "Scattering of a Bessel beam by a sphere," J. Acoust. Soc. Am. **121**, 753–758 (2007).
[15]P. L. Marston, "Acoustic beam scattering and excitation of sphere resonance: Bessel beam example," J. Acoust. Soc. Am. **122**, 247–252 (2007).
[16]F. G. Mitri, "Acoustic scattering of a high-order Bessel beam by an elastic sphere," Ann. Phys. **323**, 2840–2850 (2008).
[17]H. E. Hernandez-Figeroa, M. Zamboni-Rached, and E. Recami, *Localized Waves* (IEEE, Piscataway, NJ, 2008), pp. 7–34.
[18]M. Abramowitz and I. A. Stegun, *Handbook of Mathematical Functions* (National Bureau of Standards, Washington, DC, 1972), pp. 253–478.
[19]J. A. Stratton, *Electromagnetic Theory* (McGraw-Hill, New York, 1941), p. 413.
[20]L. V. King, "On the acoustic radiation pressure on spheres," Proc. R. Soc. London Ser. A **137**, 212–240 (1935).
[21]T. F. W. Embleton, "Mean force on a sphere in a spherical sound field. I. Theoretical," J. Acoust. Soc. Am. **26**, 40–45 (1954).
[22]K. Yosioka and Y. Kawasima, "Acoustic radiation pressure on a compressible sphere," Acoustica **5**, 167–173 (1955).
[23]X. Chen and R. E. Apfel, "Radiation force on a spherical object in an axisymmetric wave field and its application to the calibration of high-frequency transducers," J. Acoust. Soc. Am. **99**, 713–724 (1996).
[24]R. Hickling, "Analysis of echoes from a solid elastic sphere in water," J. Acoust. Soc. Am. **34**, 1582–1592 (1962).
[25]R. H. Hackman and G. S. Sammelmann, "On the existence of the Rayleigh wave dipole resonance," J. Acoust. Soc. Am. **85**, 2284–2289 (1989).
[26]R. H. Vogt and W. G. Neubauer, "Relationship between acoustic reflection and vibrational modes of elastic spheres," J. Acoust. Soc. Am. **60**, 15–22 (1976).
[27]L. Flax, L. R. Dragonette, and H. Uberall, "Theory of elastic resonance excitation by sound scattering," J. Acoust. Soc. Am. **63**, 723–731 (1978).
[28]K. L. Williams and P. L. Marston, "Synthesis of backscattering from an elastic sphere using the Sommerfeld-Watson transformation and giving a Fabry-Perot analysis of resonances," J. Acoust. Soc. Am. **79**, 1702–1708 (1986).
[29]P. L. Marston, "GTD for backscattering from elastic spheres and cylinders in water and the coupling of surface elastic waves with the acoustic field," J. Acoust. Soc. Am. **83**, 25–37 (1988).
[30]B. T. Hefner and P. L. Marston, "Backscattering enhancements associated with subsonic Rayleigh waves on polymer spheres in water: Observation and modeling for acrylic spheres," J. Acoust. Soc. Am. **107**, 1930–1936 (2000).
[31]A. N. Norris, "Resonant acoustic scattering from solid targets," J. Acoust. Soc. Am. **88**, 505–514 (1990).

Redistribution subject to ASA license or copyright; see http://acousticalsociety.org/content/terms. Download to IP: 137.222.120.226 On: Wed, 06 Apr 2016 13:18:52